Multifocal noncontact color imaging for depth-sensitive fluorescence measurements of epithelial cancer

Caigang Zhu,† Yi Hong Ong,† and Quan Liu*

Division of Bioengineering, School of Chemical and Biomedical Engineering, Nanyang Technological University, Singapore 637457, Singapore
**Corresponding author: quanliu@ntu.edu.sg*

Received February 25, 2014; revised March 29, 2014; accepted April 21, 2014;
posted April 22, 2014 (Doc. ID 207177); published May 26, 2014

We propose a multifocal noncontact setup to perform depth-sensitive fluorescence imaging on a two-layered epithelial tissue model. The combination of a microlens array and a tunable lens enables the depth of the multifocal plane to be conveniently adjusted without any mechanical movement of the imaging lens or the sample. This advantage is particularly desirable in the clinical setting. Results from the phantom study demonstrate that the setup can achieve depth-sensitive color imaging for fluorescence measurements, which is further confirmed by spectral measurements. © 2014 Optical Society of America

OCIS codes: (110.0113) Imaging through turbid media; (110.2945) Illumination design; (170.6510) Spectroscopy, tissue diagnostics.
http://dx.doi.org/10.1364/OL.39.003250

Depth-sensitive optical spectroscopy has attracted an increasing interest for the diagnosis of epithelial cancers in the past years [1–3]. Because the distribution of molecules such as endogenous fluorophores in epithelial tissues is depth dependent and varies significantly with disease stage [4], depth-sensitive optical measurements may yield higher sensitivity to malignant growth in epithelial tissues than common optical measurements in which optical signals are averaged throughout the volume being interrogated. A common setup for optical spectroscopy uses a fiber-optic probe for the delivery of illuminating light and collection of emitted light [5,6]. In a fiber-optic spectroscopy setup it is possible to achieve depth-sensitive measurements by varying the source-detector separation [2], the effective aperture diameter of fibers [1], and the illumination and collection angles [4]. However, the uncertainty in measurements due to inconsistent probe-sample pressure could induce significant distortion in measured spectra, which consequently would cause large errors in diagnosis [7]. Lens based setups have been investigated to perform noncontact optical measurements to overcome this problem. Andree *et al.* [8] performed spatially resolved diffuse reflectance measurements without physically contacting a tissue sample by using a noncontact setup. The setup involved a spherical and a flat folding mirror for illumination, while two achromatic lenses were used for detection. Bish *et al.* [9] achieved noncontact diffuse reflectance measurements on tissue phantoms and human skin by a lens based noncontact probe. Mazurenka *et al.* [10] pursued time-resolved diffuse reflectance measurements by a noncontact-lens based setup in which laser scanning was used to achieve imaging. Although these reports addressed the problem of inconsistent probe-sample contact, none of them are suitable for depth-sensitive measurements because of the lack of change in the depth of light focus. Our previous numerical study [11] demonstrated that it is possible to use a lens-based noncontact setup to obtain depth-sensitive diffuse reflectance measurements on an epithelial cancer model by adjusting the depth of light focus under the tissue surface. We also developed a special lens-based noncontact setup [3] for point measurements to achieve depth-sensitive fluorescence spectroscopy on a human skin model without moving the imaging lens or sample. Unfortunately, most above setups were designed for point measurements, which is slow when optical imaging in a large field of view is desired. This is especially true in the diagnosis of early epithelial cancer where the spatial context in optical images may provide important information for clinical diagnosis. In this report we demonstrate a multifocal noncontact setup to perform depth-sensitive fluorescence imaging on tissue phantoms in a large field of view for the diagnosis of early epithelial cancer. Moreover our setup does not require the mechanical movement of any optical components or sample to achieve depth-sensitive optical measurements and thus would be convenient in the clinical setting.

The schematic of our proposed setup is shown in Fig. 1. In the illumination module, a 405 nm laser (iFlex-2000, Point Source Ltd., Hamble, UK) with a maximum output power of 20 mW was used as the excitation source. The laser light was coupled onto a beam expander to achieve a beam diameter of 4 mm before passing through a dichroic mirror. Next to the dichroic mirror a microlens

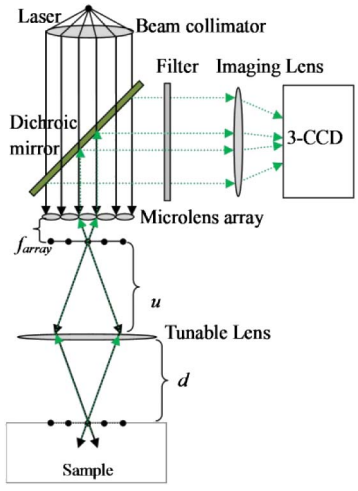

Fig. 1. Schematic of the multifocal noncontact imaging setup. Solid lines with arrows represent excitation light flow while green dotted lines represent emission light flow. Light propagation is illustrated for one microlens only in the region below the microlens array for clarity.

array was used to generate a multifocal plane for illumination, which was imaged onto a tissue sample by a tunable lens (HR EL-10-30, Optotune, Dietikon, Switzerland). The microlens array (Customized model, Wuxi Opton Tech Ltd., Jiang Su, China) contained around 20×20 microlenses and each single microlens had a diameter of 250 μm and a focal length of 1000 μm. The filling factor of the microlens array was around 75%. The focal length of the tunable lens can be varied precisely by changing the current applied to it. When the focal length of the tunable lens was changed, the depth of the focal plane of the microlens array under the sample surface, which will be named as the focal depth in the rest of the Letter, would vary accordingly. With the help of the tunable lens, the focal depth inside the sample can be varied easily and precisely without any mechanical movement of the imaging lens or the sample.

In the detection module, fluorescence from the sample was first imaged onto the microlens array's focal plane by the tunable lens. It was then defocused by the microlens array, deflected by the dichroic mirror toward a long-pass filter, and finally imaged by a convex lens onto a color camera (AT-200 GE, JAI, San Jose, California) equipped with 3-CCD. The camera captured images in red, green and blue channels. The distance between the focal plane of the microlens array and tunable lens, labeled as u in Fig. 1, was fixed at 5.5 cm, while the distance between the sample surface and tunable lens, labeled as d in Fig. 1, was set to 4.5 cm. The focal length of the tunable lens varied from 2.45 to 2.60 cm with an increment around 0.25 mm. Consequently, it can be calculated that the focal depth was varied from −0.8 to 5.2 mm approximately with an increment of 0.8 mm, assuming that the sample surface corresponded to a focal depth of zero. It should be noted that the filling factor of the microlens array we used is only 75%, which means that a considerable portion of excitation light passing through the array would stay parallel. It was necessary to reduce this portion of excitation light hitting the tunable lens; otherwise it would form a strong focal spot after passing through the tunable lens and serve as the background in the subsequent depth-sensitive measurements. In order to solve this problem, a blocker made of aluminum foil with a diameter of around 4.0 mm was placed immediately above the tunable lens to block the parallel light. The distance between the microlens array and tunable lens in our setup was large enough so that the portion of light focused by the microlenses formed a light beam 10 mm in diameter on the top surface of the tunable lens. The portion of parallel light remained 4 mm in diameter on the same surface. This ensured that all parallel light has been effectively blocked. It should be noted that a small amount of focused light from the microlens array was also blocked, but the major portion of focused light passing through was sufficient for fluorescence imaging.

The setup was evaluated on a two-layered agar tissue phantom. The phantom was prepared following the procedure published in an earlier publication [12] in which the optical properties were representative of human epithelial tissues. The thickness of the top layer was 500 μm. The thickness of the bottom layer was 1 cm and the lateral dimensions of both layers were larger than 3 cm, which were large enough to represent a semi-infinite medium. Protoporphyrin IX (PpIX) was added into the top layer at a concentration of 71.1 μM while flavin adenine dinucleotide (FAD) was added into the bottom layer at a concentration of 25.5 μM. PpIX and FAD, which can be found in the skin, were chosen in this study because their nonoverlapping emission peaks were located at 670 and 530 nm, respectively. Thus it would be easy to discriminate fluorescence signals originating from different layers. The concentrations of two fluorophores were chosen so that the magnitudes of both emission peaks fell within the same order. Polystyrene spheres (07310, Polysciences, Warrington, Pennsylvania) and Nigrosin (N4754, Sigma-Aldrich, St. Louis, Missouri) were added into each layer at a different concentration to mimic the light scattering and absorption properties of the epithelium and stroma in cervical tissues at 530 nm [13]. A plastic wrap about 10 μm in thickness was used to separate the top and bottom layers to prevent the diffusion of fluorophores and nigrosin molecules from crossing the interface between the two layers. The optical properties of the top and bottom layers in the tissue phantom at the excitation wavelength and the peak emission wavelengths of FAD and PpIX are listed in Table 1.

All experiments were performed in a dark room. The focal length of the tunable lens was controlled precisely by changing the current applied via the software provided by the manufacturer. Within the range of the tunable lens' focal length, a total of eight color images were acquired, one image for each focal depth taking 1 s. There was a 10 s time interval between two consecutive measurements to minimize photo bleaching. The acquired color images were processed using ImageJ software first to pick up the regions of interest and then further processed by a custom programmed image processing code written in Matlab (R2010, MathWorks, USA).

A sequence of color images with different focal depths are shown in Fig. 2(a). In each subfigure of Fig. 2(a), every circular bright spot refers to one focal spot imaged from the surface or the inside of the tissue phantom. When the focal depth was varied from 0 (i.e., tissue surface) to 4.3 mm, slight color changes can be observed. As the light focus moved deeper, the bright spots gradually varied from faint red to faint green. This trend was more obvious in the color values shown in Fig. 2(b), in which the color values in nine different focal regions were averaged to calculate the mean and standard deviation. It can be seen clearly that when the focal depth was increased from −0.8 to 5 mm, both the R and G values increased to their peak first and then decreased. However the R value (mainly from PpIX in the top layer) reached the peak earlier than the G value (mainly from FAD in the bottom layer). Moreover, the R value de-

Table 1. Optical Properties of Tissue Phantom [13][a]

	405 nm (Excitation)		530 nm (FAD)		670 nm (PpIX)	
	μ_a	μ_s	μ_a	μ_s	μ_a	μ_s
Top layer	1.2	39.7	1.9	34.2	1.8	23.1
Bottom layer	1.4	250.2	2.2	215.1	2.1	174.0

[a] μ_a, absorption coefficient in cm^{-1}; μ_s, scattering coefficient in cm^{-1}.

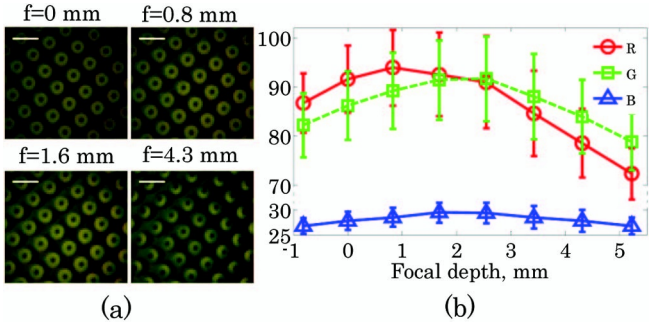

Fig. 2. (a) Color images acquired at different focal depths. (b) Raw RGB values averaged for bright spots at a range of focal depths. The scale bar represents 400 μm.

creased faster than G value. This observation directly demonstrated that our setup was capable of discriminating fluorescence from various depths with different sensitivities, which is essential in depth-sensitive fluorescence imaging. The B value was relatively low and changed very little with the focal depth as compared to the R and G values. This was due to the fact that the two selected fluorophores in this report contributed little to the blue channel and most blue light was blocked by the long pass filter. It is interesting to see that the signal from the top layer, i.e., the R value shown in Fig. 2(b), does not reach the maximum until the focal depth is increased to 0.8 mm, which is slightly larger than the thickness of top layer (note that the data points between 0 and 0.8 mm are not shown for clear visualization). This is likely because the top layer had a considerably large scattering coefficient that could have affected the distribution of excitation light.

To characterize the depth sensitivity of the new setup, the percentage of each of R, G, and B values relative to the summation of all was calculated as shown in Fig. 3. Since the B value changed very little, only the percentages of R and G are shown. Figure 3 shows that the percentage of the R value increased a little bit when the focal plane was moved from the air to the tissue surface, then decreased all the way when the focal plane went deeper from the tissue surface to the bottom layer. In contrast, the percentage of G has the opposite trend. The trends of these ratios explained why the color of the images in Fig. 2(a) changed from faint red to faint green when the focal depth increased. The percentage change as a function of focal depth was mainly affected by the numerical aperture of the microlens array, which was 0.14 in our setup. Each single microlens can be treated as an objective lens. It is well known that an objective lens with larger numerical aperture possesses a stronger focusing power, thus such a lens would yield a better spatial resolution. Similarly a microlens array with a larger numerical aperture should yield better depth sensitivity because of the stronger focusing power. As a matter of fact, we also tried another microlens array with a smaller numerical aperture (MLA150-5C, Thorlabs, Sterling, Virginia) and found that this microlens array has much smaller depth sensitivity (results not shown in the manuscript), which demonstrated that the percentage change could be much greater if the microlens array with a considerably larger numerical aperture was used.

To clarify the source of color changes shown in the Fig. 2, fluorescence spectra were measured from the same phantom using a setup similar to that in Fig. 1, except for two differences. The first difference was that the 3-CCD was replaced by a spectrometer (QE 65 Pro, Ocean Optics, Dunedin, Florida). The second difference was that a 100 μm pinhole was placed above the microlens array to select only one microlens for illumination and detection. The exposure time used for each measurement was 2 s, and a total of eight spectra were acquired. Detected fluorescence spectra for the same range of focal depths as in Fig. 3 are shown in Fig. 4. It is interesting to see that the PpIX emission peak, around 670 nm, and the FAD emission peak, around 530 nm, both increased to their maximum first and then decreased when the focal depth increased. The PpIX emission peak reached its maximum when the focal depth was 0.80 mm, while the FAD emission peak reached its maximum later when the focal depth was 1.68 mm. The change in the intensity of PpIX peak was more dramatic than that of FAD peak, most likely because the PpIX was in the top layer. It is straightforward to see that the trend in the changes of fluorescence peaks in Fig. 4 agreed very well with those of color values as shown in Fig. 2(b).

Results shown in Fig. 2(a) demonstrated that our setup was able to acquire multifocal color images rapidly. Moreover, Figs. 2(b) and 3 showed that depth-sensitive optical imaging could be achieved in our setup by varying the focal distance of the tunable lens and in turn the depth of the multifocal plane in the sample. Color values of tissues could be used directly for cancer diagnosis [14] or to reconstruct the full spectrum using published algorithms [15,16]. Therefore our setup could potentially achieve rapid depth-sensitive spectral imaging that would

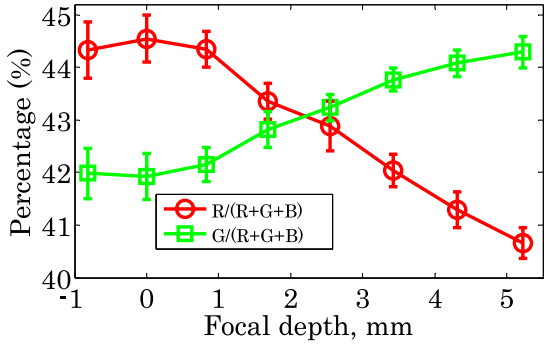

Fig. 3. Percentage of R and G values as a function of focal depth.

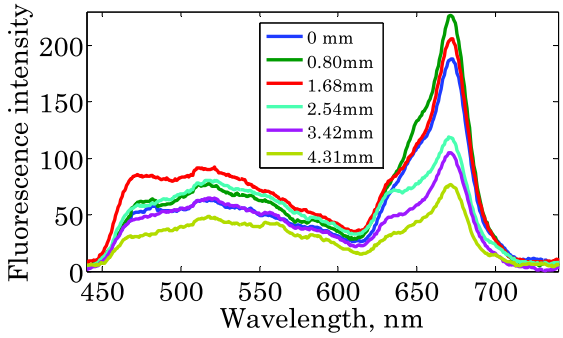

Fig. 4. Fluorescence spectra for a range of focal depths, the legend shows the values of focal depths.

be faster and cheaper than the traditional spectral imaging setup. Currently, most spectral imaging setups utilize uniform illumination [17], which induces no changes in depth sensitivity. Our setup would thus offer the advantage of variable depth sensitivity for epithelial cancer diagnosis. Another advantage of our proposed setup is the lower requirement on the excitation laser power because the excitation power is focused only on a finite number of focal spots rather than the entire tissue area.

The field of view of our setup was around 4 mm in diameter, which was limited by the size of the microlens array and the tunable lens we used. In the 4 mm field of view, totally around 10×10 microlenses were covered, which corresponded to a spatial resolution of around 0.4 mm. Note that the spatial resolution could be easily improved by changing the distances u and d in Fig. 1 or using a microlens array with smaller individual microlenses.

Another potential issue in this setup worth discussing is the variation in the focal length of the tunable lens with light wavelength, i.e., chromatic aberration. By using the law for the approximation of focal length for thick lenses [18], it was found that the focal length of the tunable lens changed 4% when the wavelength was varied from 405 to 670 nm. In our fluorescence imaging setup, chromatic aberration should not be an issue because all fluorescence light was excited by the same laser beam with a single excitation wavelength. The variation in the focal length of the tunable lens with wavelength would only result in difference in the detection efficiency in a range of emission wavelengths but not the depth of the excitation light focus. However, chromatic aberration cannot be ignored in a diffuse reflectance imaging setup since the illumination light would also contain a range of wavelengths.

In summary, we proposed a multifocal noncontact setup for depth-sensitive optical imaging on a two-layered epithelial tissue model. The setup contains a microlens array and a tunable lens, which enable the adjustment of the imaging depth without the mechanical movement of any optical components or sample. This feature would facilitate its applications in clinical setting. While color values demonstrate relatively small depth sensitivity, they could be used to reconstruct full optical spectra using the previous algorithms [15,16], which have shown much larger depth sensitivity in this study.

We gratefully acknowledge the financial support from Tier 1 grant (No. RG47/09) and Tier 2 grant (No. MOE 2010-T2-1-049), funded by the Ministry of Education, as well as NRF POC grant (No. NRF2012NRF-POC001-015) in Singapore.

†The authors have equal contribution to this manuscript.

References

1. Q. Liu and N. Ramanujam, Opt. Lett. **27**, 104 (2002).
2. T. J. Pfefer, L. S. Matchette, A. M. Ross, and M. N. Edigeret, Opt. Lett. **28**, 120 (2003).
3. Y. H. Ong and Q. Liu, Opt. Lett. **38**, 2647 (2013).
4. Q. Liu and N. Ramanujam, Opt. Lett. **29**, 2034 (2004).
5. U. Utzinger and R. R. Richards-Kortum, J. Biomed. Opt. **8**, 121 (2003).
6. Q. Liu, G. Grant, J. J. Li, Y. Zhang, F. Y. Hu, S. Q. Li, C. Wilson, K. Chen, D. Bigner, and T. Vo-Dinh, J. Biomed. Opt. **16**, 037004 (2011).
7. Y. L. Ti and W. C. Lin, Opt. Express **16**, 4250 (2008).
8. S. Andree, C. Reble, J. Helfmann, I. Gersonde, and G. Illing, J. Biomed. Opt. **15**, 067009 (2010).
9. S. F. Bish, N. Rajaram, B. Nichols, and J. W. Tunnell, J. Biomed. Opt. **16**, 120505 (2011).
10. M. Mazurenka, A. Jelzow, H. Wabnitz, D. Contini, L. Spinelli, A. Pifferi, R. Cubeddu, A. D. Mora, A. Tosi, F. Zappa, and R. Macdonald, Opt. Express **20**, 283 (2012).
11. C. G. Zhu and Q. Liu, Opt. Express **20**, 29807 (2012).
12. R. Cubeddu, A. Pifferi, P. Taroni, A. Torricelli, and G. Valentini, Phys. Med. Biol. **42**, 1971 (1997).
13. D. Arifler, C. MacAulay, M. Follen, and R. Richards-Kortum, J. Biomed. Opt. **11**, 064027 (2006).
14. K. Yamauchi, M. Yang, P. Jiang, N. Yamamoto, M. Xu, Y. Amoh, K. Tsuji, M. Bouvet, H. Tsuchiya, K. Tomita, A. R. Moossa, and R. M. Hoffman, Cancer Res. **65**, 4246 (2005).
15. J. L. Nieves, E. M. Valero, J. Hernandez-Andres, and J. Romero, Appl. Opt. **46**, 4144 (2007).
16. S. Chen and Q. Liu, J. Biomed. Opt.**17**, 030501 (2012).
17. Q. Liu, K. Chen, M. Martin, A. Wintenberg, R. Lenarduzzi, M. Panjehpour, B. F. Overholt, and T. Vo-Dinh, Opt. Express **15**, 12583 (2007).
18. F. Jenkins and H. White, in *Fundamentals of Optics* (McGraw-Hill, 1957), Chap. 5.